Available online at www.sciencedirect.com
ScienceDirect
Ceramics International 35 (2009) 441–445
CERAMICS INTERNATIONAL
www.elsevier.com/locate/ceramint

Synthesis of negative thermal expansion materials $ZrW_{2-x}Mo_xO_8$ $(0 \leq x \leq 2)$ using hydrothermal method

Juan Yang *, Qinqin Liu, Xiujuan Sun, Guifang Xu, Xiaonong Cheng

School of Materials Science & Engineering, Jiangsu University, Zhenjiang, Jiangsu 212013, PR China

Received 26 June 2007; received in revised form 4 September 2007; accepted 3 December 2007
Available online 8 April 2008

Abstract

Negative thermal expansion materials $ZrW_{2-x}Mo_xO_8$ $(0 \leq x \leq 2)$ have been successfully synthesized by the reaction of a mixture of ammonium tungstate and ammonium molybdate with zirconium oxynitrate using a hydrothermal method. Effect of substituted ion Mo on the microstructure, α-to-β and cubic to trigonal phase transition in resulting $ZrW_{2-x}Mo_xO_8$ powders was examined by the XRD experiments. It was found that the structural phase transition temperature decreased slightly with increasing substituted content. The cubic to trigonal phase transition was also influenced by substituted content. The resulting products decomposed to WO_3/MoO_3 and ZrO_2 as temperature increasing when $x \leq 0.5$ and while $x > 0.5$, the cubic phase transited to trigonal phase. The effect of substituted Mo on the morphology of resulting products was also investigated by SEM experiments.

Keywords: A. Powders: chemical preparation; B. Microstructure-final; C. Thermal expansion

1. Introduction

Materials that exhibit negative thermal expansion (NTE) are of considerable scientific and technological interest [1–3]. The most potential application is using them in composites to facilitate the control of bulk thermal expansion properties to obtain a good match to other system components or zero expansion in fields where exact positioning of parts is crucial [4–6]. The recent works on Cu/ZrW_2O_8 [7–9] and ZrW_2O_8/ZrO_2 [10,11] composites are examples of this approach.

Among all the negative thermal expansion materials, cubic ZrW_2O_8 has been extensively studied because it shows isotropic negative thermal expansion behavior over the wide temperature range from 0.3 to 1050 K [12]. But for using it as fillers in composites, there are some drawbacks [13]. ZrW_2O_8 is only thermodynamically stable at high temperatures, which makes it difficult to synthesize. Due to the α-to-β phase transition, the expansion curve shows a discontinuity around 430 K and it makes the change of the linear expansion coefficient from -8.8 to $-4.9 \times 10^{-6}\ K^{-1}$. Moreover, ZrW_2O_8 undergoes a phase transition from cubic to orthorhombic structure at 0.21 GPa that is not reversible, which leads to problems during the processing and utilizing of composites under pressure.

It has been reported that cubic $ZrMo_2O_8$ displays NTE with $\alpha = -5.0 \times 10^{-6}\ K^{-1}$ between 11 and 573 K with no phase transitions and there is a phase transition between 0.7 and 2.0 GPa but is reversible, indicating that $ZrMo_2O_8$ might be advantageous for applications in composites [14,15]. Unfortunately, cubic $ZrMo_2O_8$ is metastable at all temperatures, which makes it difficult to synthesis with pure phase and thus restricts the application in making composites.

It is known that the ZrW_2O_8 forms a complete solid solution with $ZrMo_2O_8$ and the solid solution with appropriate substitute content might centralize the advantages of ZrW_2O_8 and $ZrMo_2O_8$, which might be used in composites and replace ZrW_2O_8 or $ZrMo_2O_8$. There are some papers reporting the synthesis of Mo-substituted ZrW_2O_8 [16,17], but lack of series research on the influences of substitute content on the microstructure, the phase transition, especially the morphology of the resulting products. While in making composite, particle shape might be an important consideration in both processing and using.

* Corresponding author. Tel.: +86 511 8780195; fax: +86 511 8791947.
E-mail address: yangjuan6347@ujs.edu.cn (J. Yang).

0272-8842/$34.00
doi:10.1016/j.ceramint.2007.12.006

In this paper, $ZrW_{2-x}Mo_xO_8$ $(0 \leq x \leq 2)$ powders were synthesized by hydrothermal method and the effect of substituted-Mo content on the microstructure and morphology was also studied.

2. Experimental

All the chemical reagents were of analytical grade purity without further purification. In the typical procedure, zirconium oxynitrate $[ZrO(NO_3)_2{\cdot}5H_2O]$, ammonium tungstate $[N_5H_{37}W_6O_{24}{\cdot}H_2O]$ and ammonium molybdate $[N_5H_{37}Mo_6O_{24}{\cdot}H_2O]$ were dissolved separately in distilled water according to the molar ratio of Zr:W:Mo = 1:(2 − x):x. The Zr solution was added slowly to the mixture of W and Mo solution under vigorous stirring. Then, 6 M HCl was added slowly to the above solution with continuous stirring for another 3 h. The mixture was finally loaded into a Teflon-lined Parr bomb and heated at 180 °C for 15 h followed by washing with distilled water and drying at 60 °C. To obtain pure $ZrW_{2-x}Mo_xO_8$ $(0 \leq x \leq 2)$ powders the obtained solid products (precursors) were heated at different temperatures mainly according to the TG-DSC results.

The resulting products were characterized by powder X-ray diffraction using Cu Kα radiation (λ = 0.15418 nm) with 40 kV/200 mA (D/max2500, Rigaku). The XRD data were collected with a scan speed of $5^\circ(2\theta)\ min^{-1}$ in the 2θ range from 10° to 50° by continuum scanning method. TG-DSC of the precursor was recorded on a NETZSCH-STA449.C thermogravimeter. The samples' morphology and particle size were examined with PHILIPS XL-30ESEM scanning electron microscopy.

3. Results and discussion

Fig. 1 shows the typical XRD patterns of the hydrothermal prepared $ZrW_{2-x}Mo_xO_8$ ($x = 0.3$, 1.0, 1.5) precursors. As one can see in Fig. 1, the precursors synthesized with different amount of substituted Mo ions have almost the same XRD patterns, indicating that the same products were obtained. The strong and sharp diffraction peaks appearing in the XRD diagrams have obvious relevance with the well-crystallized precursors. Other precursors with different x values obtained in the experiments also show the same XRD pattern and can be indexed as a pure $ZrW_2O_7(OH)_2(H_2O)_2$ phase (JCPDS 28-1500).

To obtain cubic $ZrW_{2-x}Mo_xO_8$, the obtained precursors must be heat-treated and the process was monitored by the TG-DSC experiments. Fig. 2(a) shows the TG-DSC curves of precursor $ZrW_{1.7}Mo_{0.3}O_7(OH)_2(H_2O)_2$. The TG curve indicates two regions of mass loss. One is from RT to 250 °C with the mass loss about 8.42% and the other is up to 900 °C. The first mass loss is mostly due to desorption of water. According to the following formula, the theoretical mass loss is 8.72% when precursor $ZrW_{1.7}Mo_{0.3}O_7(OH)_2(H_2O)_2$ is changed into $ZrW_{1.7}Mo_{0.3}O_8$, which is similar to our experimental result. The second mass loss may be due to the decomposition of the obtained $ZrW_{1.7}Mo_{0.3}O_8$ which might be confirmed by the XRD results discussed below.

$$ZrW_{1.7}Mo_{0.3}O_7(OH)_2(H_2O)_2 \rightarrow ZrW_{1.7}Mo_{0.3}O_8 + 3H_2O\uparrow$$

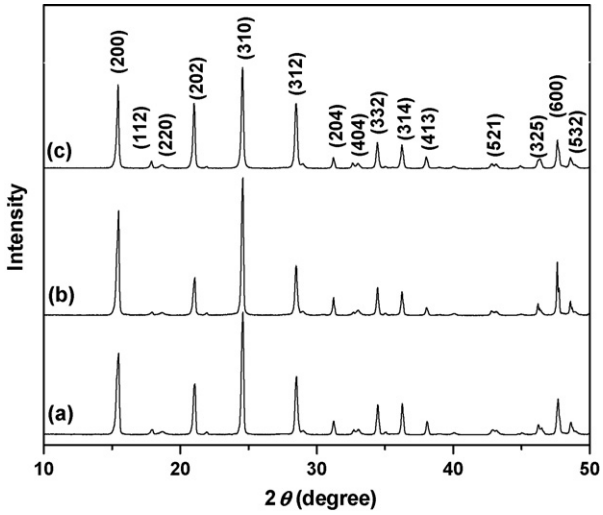

Fig. 1. XRD patterns of $ZrW_{2-x}Mo_xO_8$ precursors (a) $x = 0.3$; (b) $x = 1.0$; (c) $x = 1.5$.

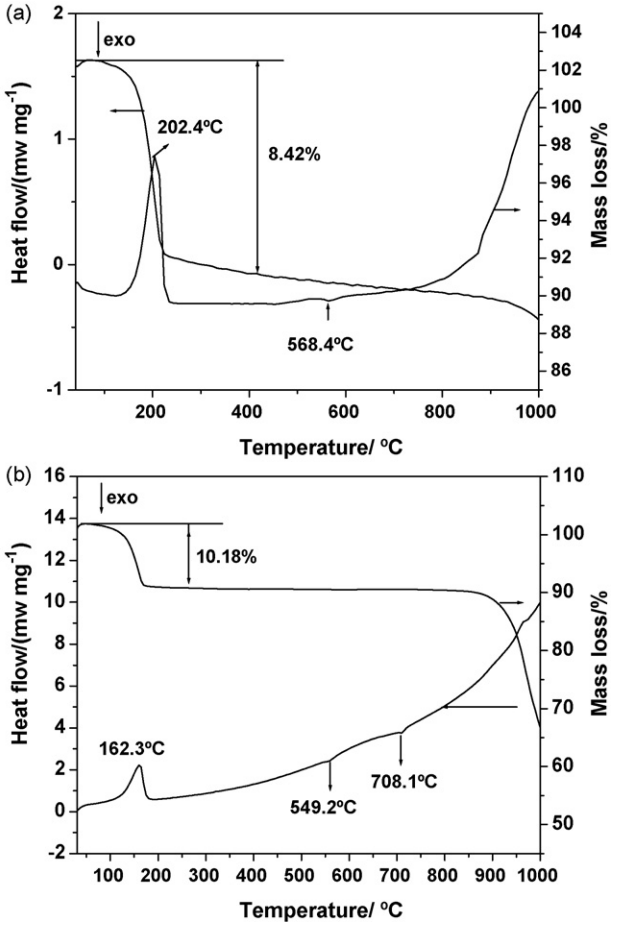

Fig. 2. TG-DSC curves of (a) precursor $ZrW_{1.7}Mo_{0.3}O_7(OH)_2(H_2O)_2$ and (b) precursor $ZrWMoO_7(OH)_2(H_2O)_2$.

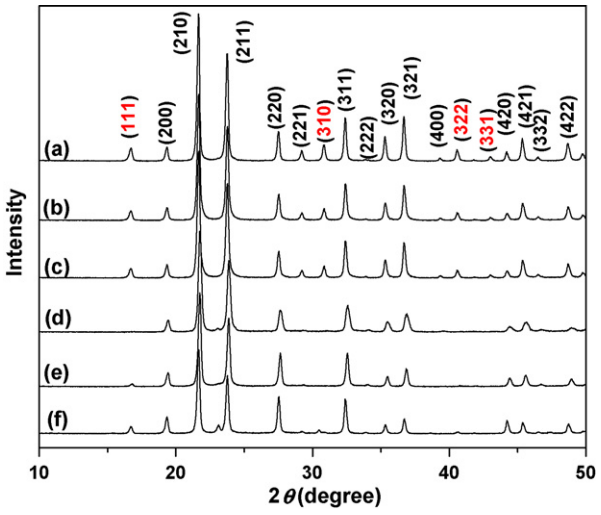

Fig. 3. XRD patterns of the obtained powders (a) ZrW_2O_8; (b) $ZrW_{1.7}Mo_{0.3}O_8$; (c) $ZrW_{1.5}Mo_{0.5}O_8$; (d) $ZrWMoO_8$; (e) $ZrW_{0.5}Mo_{1.5}O_8$; (f) $ZrMo_2O_8$.

The DSC curve reveals an endothermic peak that correlates to the first mass loss and the other endothermic peak over the temperature range of the second mass loss. There is a small exothermic peak at around 568.4 °C indicating the phase formation of cubic phase.

Fig. 2(b) shows the TG-DSC curves of precursor $ZrWMoO_7(OH)_2(H_2O)_2$. Compared with Fig. 2(a), there are two small exothermic peaks at 549.2 and 708.1 °C, which might be caused by the phase formation of cubic phase and the trigonal phase respectively and this could be confirmed by the XRD results shown in Figs. 3 and 4.

All the TG-DSC curves of different precursors are similar to Fig. 2 but with different mass loss values and different phase formation temperatures.

According to the TG-DSC results, to obtain pure cubic phase, the precursors were heat-treated at different temperatures. For $x = 0$, 0.3, 0.5, 1.0, 1.5 and 2.0, the heating temperatures are 580, 570, 550, 550, 480 and 400 °C respectively, and the XRD patterns of the resulting powders are shown in Fig. 3.

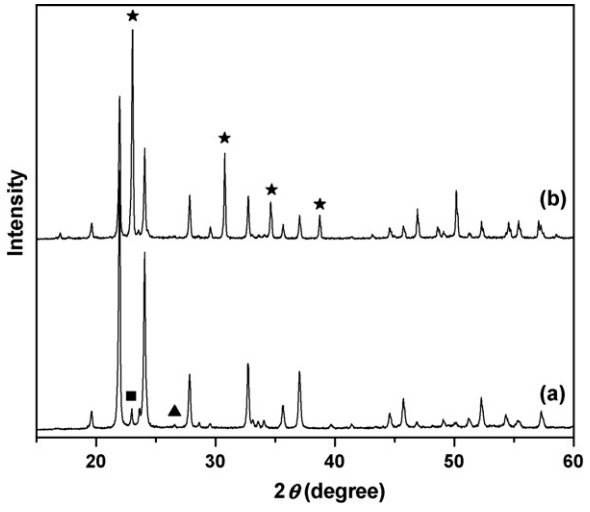

Fig. 4. XRD patterns of (a) $ZrW_{1.5}Mo_{0.5}O_8$ and (b) $ZrWMoO_8$ powders calcined at 700 °C (■: WO_3; ▲: ZrO_2; ★: trigonal $ZrWMoO_8$).

In Fig. 3, it can be seen that all the products are showing high and sharp diffraction peaks which indicates the good crystallinity of all the obtained powders. There are some differences between the XRD patterns with carefully comparison. The XRD patterns of samples ZrW_2O_8, $ZrW_{1.7}Mo_{0.3}O_8$ and $ZrW_{1.5}Mo_{0.5}O_8$ (Fig. 3(a)–(c)) are the same and display the characteristic XRD peaks corresponding to α-ZrW_2O_8 (JCPDS(13-0557), space group: $P2_13$), no obvious diffraction peaks arising from the possible impurity phases such as WO_3, ZrO_2, etc. are visible. When the substituting ion increased (e.g. $x = 1$), peaks (1 1 1), (3 1 0), (3 2 2) and (3 3 1) are disappeared as shown in Fig. 3(d). The remaining peaks can be indexed to β-ZrW_2O_8 (space group: $Pa\bar{3}$). The XRD patterns of samples $ZrW_{0.5}Mo_{1.5}O_8$ and $ZrMo_2O_8$ are almost the same but are different with those of $ZrWMoO_8$ or ZrW_2O_8. Compared with Fig. 3(a), only (3 1 0), (3 2 2) and (3 3 1) peaks are disappeared but peak (1 1 1) still exists. According to literature [18], this is a pure cubic $ZrMo_2O_8$ phase. Usually, cubic ZrW_2O_8 obtained at room temperature shows α-ZrW_2O_8 structure consisting of ZrO_6 octahedra linked through oxygen atoms with WO_4 tetrahedra. There is a kinetically limited order–disorder phase transition at about 430 K, and above this temperature, the structure of ZrW_2O_8 is changed into a disordered phase β-ZrW_2O_8 with one oxygen site half occupied. According to the XRD results discussed above, it can be concluded that the order–disorder transformation is also affected by the substituted content of Mo and the α–β phase transition temperature decreased slightly with increasing the content of Mo, which is in accordance with the result reported by Evans et al. [19].

In $ZrW_{2-x}Mo_xO_8$ system, the structure of the obtained products can be adjusted between α-ZrW_2O_8 to β-ZrW_2O_8 or to cubic $ZrMo_2O_8$ simply by changing the x values in our experiments.

To investigate the heat stability of the obtained powders, $ZrW_{2-x}Mo_xO_8$ ($0 \leq x \leq 2$) were calcined at different temperatures and the structures were characterized by XRD. Fig. 4 shows the typical XRD patterns of $ZrW_{1.5}Mo_{0.5}O_8$ and $ZrWMoO_8$ calcined at 700 °C. It can be found that after heat-treated at 700 °C, $ZrW_{1.5}Mo_{0.5}O_8$ was decomposed and slight amount of WO_3 and ZrO_2 were detected as shown in Fig. 4(a). While in Fig. 4(b), $ZrWMoO_8$ with trigonal phase is visible and these results are in accordance with TG-DSC analyses. In our experiments, it was found that the resulting products with $x \leq 0.5$ would decompose to WO_3/MoO_3 and ZrO_2 as temperature increasing, while $x > 0.5$, the cubic phase would transit to trigonal phase.

The negative thermal expansion property of the obtained samples was investigated by the cell parameter calculation method together with the thermal mechanical analysis and the results indicate that all the samples show NTE property (e.g. the NTE coefficient of $ZrW_{1.7}Mo_{0.3}O_8$ from 20 to 700 °C is $-6.61 \times 10^{-6}\,K^{-1}$) but there are differences between them. The differences might be caused by the different microstructure and the results will be published elsewhere.

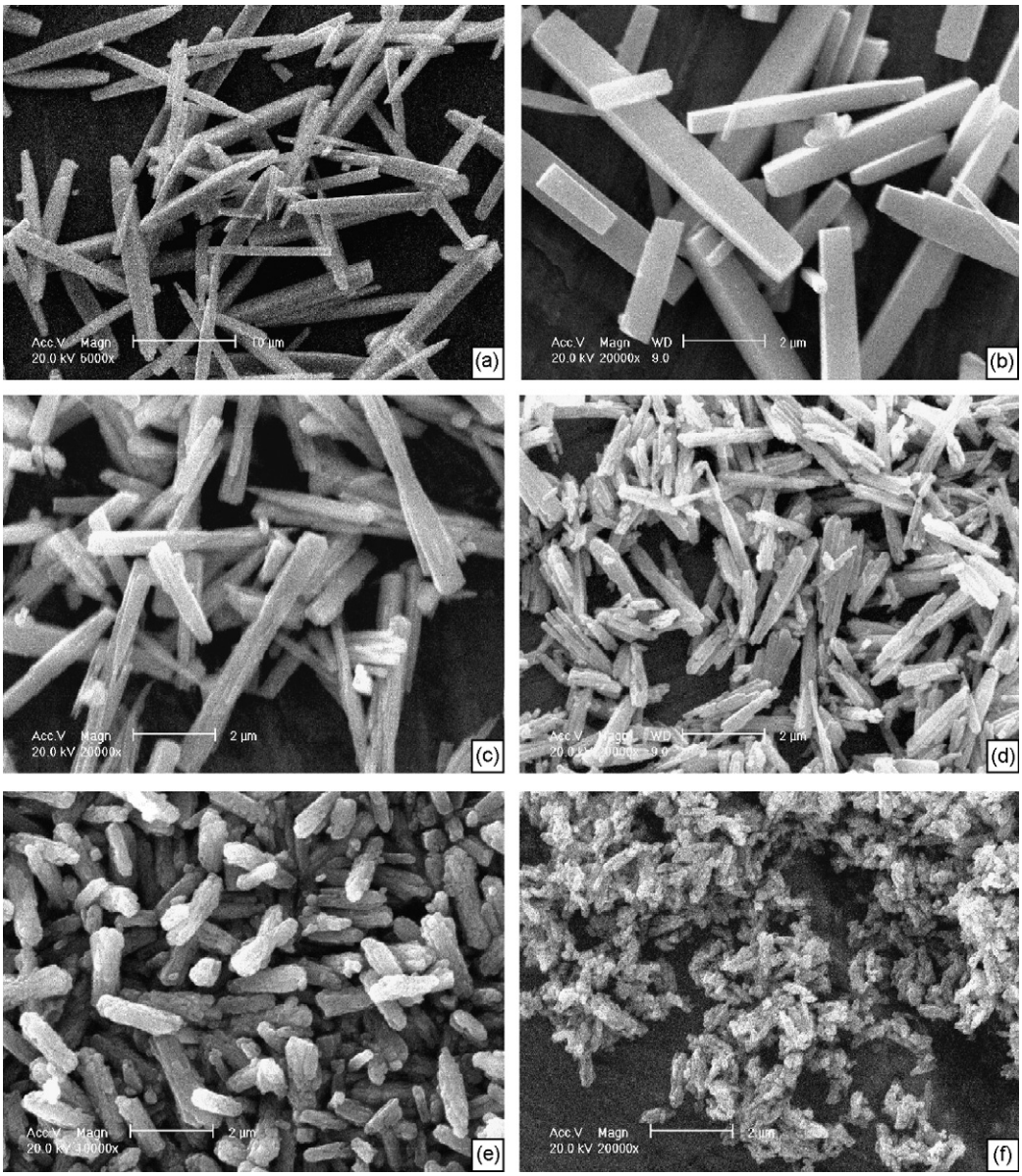

Fig. 5. SEM images of samples (a) ZrW_2O_8; (b) $ZrW_{1.7}Mo_{0.3}O_8$; (c) $ZrW_{1.5}Mo_{0.5}O_8$; (d) $ZrWMoO_8$; (e) $ZrW_{0.5}Mo_{1.5}O_8$; (f) $ZrMo_2O_8$.

More interestingly, $ZrW_{2-x}Mo_xO_8$ $(0 \leq x \leq 2)$ powders with different x values have different morphologies. The SEM images of $ZrW_{2-x}Mo_xO_8$ ($x = 0, 0.3, 0.5. 1.0, 1.5, 2.0$) are listed in Fig. 5.

ZrW_2O_8 powders which were prepared by hydrothermal method show rod-like (2 μm wide) appearance with lengths exceeding to 10 μm (Fig. 5(a)). In Fig. 5(b), it can be seen that the substituting small amount of Mo produces regular rods of very smooth facets with the wideness of about 800 nm and the lengths of 5 μm. While the substituting Mo ions increased ($x \geq 0.5$), the rod-like morphology was changed. The as-prepared particles of $ZrW_{1.5}Mo_{0.5}O_8$ and $ZrWMoO_8$ appeared rod-like aggregates and the aggregates were made up of several nanorods which connected with each other to form a bundle of nanorods with rod-like morphology (Fig. 5(c) and (d)). The lengths of the rod-like aggregates were 4 and 2 μm respectively. In Fig. 5(e), one can see that the morphology was changed to peanut-like aggregates which were also made up by several nanorods but the lengths were reduced to about 1.8 μm. When the W was completely substituted by Mo, the obtained $ZrMo_2O_8$ powders were nanorod-like with average wideness of 50 nm and lengths of 500 nm. From the SEM results, it can be concluded that the sizes and morphologies of $ZrW_{2-x}Mo_xO_8$ powders were extensively influenced by the molar ratio of W/Mo. With the increase of Mo, the particle sizes were decreased and the mechanism needs further investigation.

4. Conclusion

A series of $ZrW_{2-x}Mo_xO_8$ $(0 \leq x \leq 2)$ powders were successfully prepared using hydrothermal method followed by heat-treatment. The influences of the molar ratio of W/Mo in $ZrW_{2-x}Mo_xO_8$ $(0 \leq x \leq 2)$ system were studied in detail and it can be found that the microstructure and particle size or

morphology can be adjusted simply by changing the x values. The results reported here might have potential meanings in promoting the application of negative thermal expansion materials.

References

[1] S. Sumithra, A.M. Umarji, Negative thermal expansion in rare earth molybdates, Solid State Sci. 8 (12) (2006) 1453–1458.

[2] P. Fornasini, G. Dalba, R. Grisenti, J. Purans, M. Vaccari, F. Rocca, A. Sanson, Local behaviour of negative thermal expansion materials, Nucl. Instrum. Methods Phys. Res. B 246 (1) (2006) 180–183.

[3] Y. Yamamura, M. Kato, T. Tsuji, Synthesis and phase transition of negative thermal expansion materials $Zr_{1-x}Lu_xW_2O_{8-y}$, Thermochim. Acta 431 (1–2) (2005) 24–28.

[4] A. Kelly, R.J. Stearn, L.N. McCartney, Composite materials of controlled thermal expansion, Compos. Sci. Technol. 66 (2) (2006) 154–159.

[5] R. Stevens, J. Linford, B.F. Woodfield, J. Boerio-Goates, C. Lind, A.P. Wilkinson, G. Kowach, Heat capacities, third-law entropies and thermodynamic functions of the negative thermal expansion materials, cubic alpha-ZrW_2O_8 and cubic $ZrMo_2O_8$, from $T = (0$ to $400)$ K, J. Chem. Thermodyn. 35 (6) (2003) 919–937.

[6] A.K.A. Pryde, K.D. Hammonds, M.T. Dove, Origin of the negative thermal expansion in ZrW_2O_8 and ZrV_2O_7, J. Phys.: Condens. Matter 8 (50) (1996) 10973–10982.

[7] S. Yilmaz, D.C. Dunand, Finite-element analysis of thermal expansion and thermal mismatch stresses in a Cu–60vol%ZrW_2O_8 composite, Compos. Sci. Technol. 64 (12) (2004) 1895–1898.

[8] S. Yilmaz, Thermal mismatch stress development in Cu–ZrW_2O_8 composite investigated by synchrotron X-ray diffraction, Compos. Sci. Technol. 62 (14) (2002) 1835–1839.

[9] C. Verdon, D.C. Dunand, High-temperature reactivity in the ZrW_2O_8–Cu system, Scr. Mater. 36 (9) (1997) 1075–1080.

[10] X.B. Yang, X.N. Cheng, X.H. Yan, J. Yang, T.B. Fu, J. Qiu, Synthesis of ZrO_2/ZrW_2O_8 composites with low thermal expansion, Compos. Sci. Technol. 67 (6) (2007) 1167–1171.

[11] P. Lommens, C.D. Meyer, E. Bruneel, Synthesis and thermal expansion of ZrO_2/ZrW_2O_8 composites, J. Eur. Ceram. Soc. 25 (16) (2005) 3605–3610.

[12] J.S.O. Evans, Z. Hu, J.D. Jorgensen, D.N. Argyriou, S. Short, A.W. Sleight, Compressibility, phase transitions, and oxygen migration in zirconium tungstate, ZrW_2O_8, Science 275 (1996) 61.

[13] U. Kameswari, A.W. Sleight, J.S.O. Evans, Rapid synthesis of ZrW_2O_8 and related phases, and structure refinement of $ZrWMoO_8$, Int. J. Inorg. Mater. 2 (4) (2000) 333–337.

[14] S. Allen, N.R. Warmingham, R.K.B. Cover, Synthesis, structure and thermal contraction of a new low-temperature polymorph of $ZrMo_2O_8$, Chem. Mater. 15 (18) (2003) 3406–3410.

[15] A. Grzechnik, W.A. Crichton, Structural transformations in cubic $ZrMo_2O_8$ at high pressures and high temperatures, Solid State Sci. 4 (9) (2002) 1137–1141.

[16] T. Varga, A.P. Wilkinsona, C. Lind, W.A. Bassett, C.S. Zha, Pressure-induced amorphization of cubic $ZrMo_2O_8$ studied in situ by X-ray absorption spectroscopy and diffraction, Solid State Commun. 135 (11–12) (2005) 739–744.

[17] C. Closmann, A.W. Sleight, J.C. Haygarth, Low-temperature synthesis of ZrW_2O_8 and Mo-substituted ZrW_2O_8, J. Solid State Chem. 139 (2) (1998) 424–426.

[18] C. Lind, A.P. Wilkinson, C.J. Rawn, E.A. Payzant, Preparation of the negative thermal expansion material cubic $ZrMo_2O_8$, J. Mater. Chem. 11 (12) (2001) 3354–3359.

[19] J.S.O. Evans, P.A. hanson, R.M. Ibberson, N. Duan, U. Kameswari, A.W. Sleight, Low-temperature oxygen migration and negative thermal expansion in $ZrW_{2-x}Mo_xO_8$, J. Am. Chem. Soc. 122 (36) (2000) 8694–8699.